Synergistic Effect of Fluorinated Passivator and Hole Transport Dopant Enables Efficient and Stable Perovskite Solar Cells with Efficiency Near 24%

Hongwei Zhu[1,2,3], Yameng Ren[*2], Linfeng Pan[4], Olivier Ouellette[2], Felix T. Eickemeyer[2], Yinghui Wu[4], Xianggao Li[*1,3], Shirong Wang[1,3], Hongli Liu[1,3], Xiaofei Dong[1,3], Shaik M. Zakeeruddin[2], Yuhang Liu[*2], Anders Hagfeldt[4], and Michael Grätzel[*2]

1. Tianjin University, School of Chemical Engineering and Technology, Tianjin 300072, China

2. Laboratory of Photonics and Interfaces (LPI), Department of Chemistry and Chemical Engineering, École Polytechnique Fédérale de Lausanne, Lausanne CH-1015, Switzerland.

3. Collaborative Innovation Center of Chemical Science and Engineering, Tianjin 300072, China

4. Laboratory of Photomolecular Science (LSPM), École Polytechnique Fédérale de Lausanne, Station 6, CH-1015 Lausanne, Switzerland.

[†]Corresponding to: Dr. Yuhang Liu, yuhang.liu@epfl.ch, Dr Yameng Ren, yameng.ren@epfl.ch, Prof. Xianggao Li, lixianggao@tju.edu.cn,   Prof. Michael Graetzel, michael.graetzel@epfl.ch.

Abstract

Long-term durability is critically important for the commercialization of the advanced perovskite solar cell (PSC) technology. Since the ionic perovskite materials and the hole-transporting layer (HTL) additives customarily used, for example, lithium bis(trifluoromethanesulfonyl)imide (Li-TFSI) and *tert*-butyl pyridine(*t*BP), are intrinsically hydrophilic and the degradation of the PSCs upon moisture uptake compromises long-term stability of the PSCs, it is important to take steps to reduce their hydrophilicity. In this work, we employ a trifluoromethylation strategy to chemically functionalize the perovskite passivation layer and the HTL additive, to yield 4-trifluoromethyl-benzylammonium iodide (FBAI) as a molecular passivator and 4-(trifluoromethyl)pyridine (TFP) as a HTL additive, respectively. Surface treatment of the triple cation perovskite ($Cs_{0.05}FA_{0.85}MA_{0.10}Pb(I_{0.97}Br_{0.03})_3$) light harvester with FBAI largely suppressed the nonradiative charge carrier recombination, boosting the power conversion efficiency (PCE) from 20.9% to 23.9% with negligible hysteresis. Adding TFP into the HTL yielded strong resistance to moisture for the PSC while similar PCE compared to the standard HTL PSC devices was maintained. When

combining FBAI surface passivation with adding TFP into the HTL, our new synergistic approach successfully increased the PSC device's hydrophobicity through fluorination of both the HTL additive and the passivation material, leading to FBAI/TFP based PSCs retaining over 96% of their initial efficiency after 500 h maximum power point tracking (MPPT) under simulated full-sun irradiation, and 97% of their initial efficiency after 1100 h storage under ambient condition at a relative humidity (*r.h.*) of 60 - 70%.

Introduction

During the past decade the development of perovskite solar cells (PSCs) has become a game-changer in the field of photovoltaics with relatively rapid progress in the attainment of power conversion efficiencies (PCEs) of over 25%[1-5]. Along with the fundamental breakthroughs, the commercialization of PSCs has been advanced. Improvement in the stability of PSC devices remains the most challenging issue[6-10] to this PV technology. The best performing PSCs are mostly based on a n-*i*-p device structure, where n refers to *n*-type semiconductor, normally TiO_2[11; 12] or SnO_2[13; 14]. The organic-inorganic lead halide perovskite used as the light-absorbing layer is sandwiched between the electron transporting layer (ETL) and the hole transporting layer (HTL) for selective charge carrier extraction. Since the ETL is deposited in-between the transparent conductive substrate (e.g. fluorine doped tin oxide (FTO) or indium doped tin oxide (ITO).) and the perovskite active layer, water and oxygen ingression from the environment destroys the PSCs mainly at the perovskite/HTL interface[15; 16]. Ambient moisture uptake is one of the key issues resulting in poor operational stability of the PSCs due to the intrinsic hydrophilicity of the perovskite active layer materials[17; 18]. In addition, the widely used HTL additives, such as (lithium bis(trifluoromethanesulfonyl)imide (Li-TFSI) and *tert*-butyl pyridine (*t*BP)), are hydrophilic, intensifying moisture penetration from ambient air to the perovskite through the HTL[19-22]. Liu et al[23] reported that the use of fluorinated phenylethylammonium iodide can greatly enhanced i the hydrophobicity of the perovskite, improving operational stability against moisture. However, the effect of the hydrophobic HTL additives on the PCE and the long term stability has remained less explored.

In this work, we firstly applied a novel trifluoromethylated interface passivation material, 4-

trifluoromethyl-benzylammonium iodide (FBAI), to augment the hydrophobicity of the Cs$_{0.05}$FA$_{0.85}$MA$_{0.10}$Pb(I$_{0.97}$Br$_{0.03}$)$_3$ triple cation perovskite while simultaneously suppressing the defects. The perovskite film passivated with FBAI exhibits a much higher photoluminescence quantum yield (PLQY) and lower V_{OC} loss against the radiative limit compared with the pristine film (**Figure 3d**), revealing the excellent passivation effect of FBAI. Then, in order to increase the hydrophobicity of the triple cation perovskite active layer and the HTL layer while maintaining the high efficiency of the spiro-OMeTAD/tBP system, we modified spiro-OMeTAD HTL by adding the fluorinated additive, TFP. Time-resolved photoluminescence (TRPL) measurements and external photoluminescence quantum efficiencies (PLQY$_{ext}$) show that the introduction of TFP does not alter the extraction of holes and recombination processes at perovskite/spiro-OMeTAD interface (**Figure S8** and **S9**). A champion PSC device based on perovskite/FBAI/(spiro-OMTAD/TFP) obtained an outstanding V_{OC} of 1.163 eV, with a low voltage loss of 387 mV. Remarkably, FBAI/TFP based PSCs retain over 96% of their initial efficiency after 500 h maximum power point tracking (MPPT) under simulated full-sun irradiation and 97% of their initial efficiency after 1100 h under ambient condition at a relative humidity (*r.h.*) of 60 - 70%.

Results and discussion
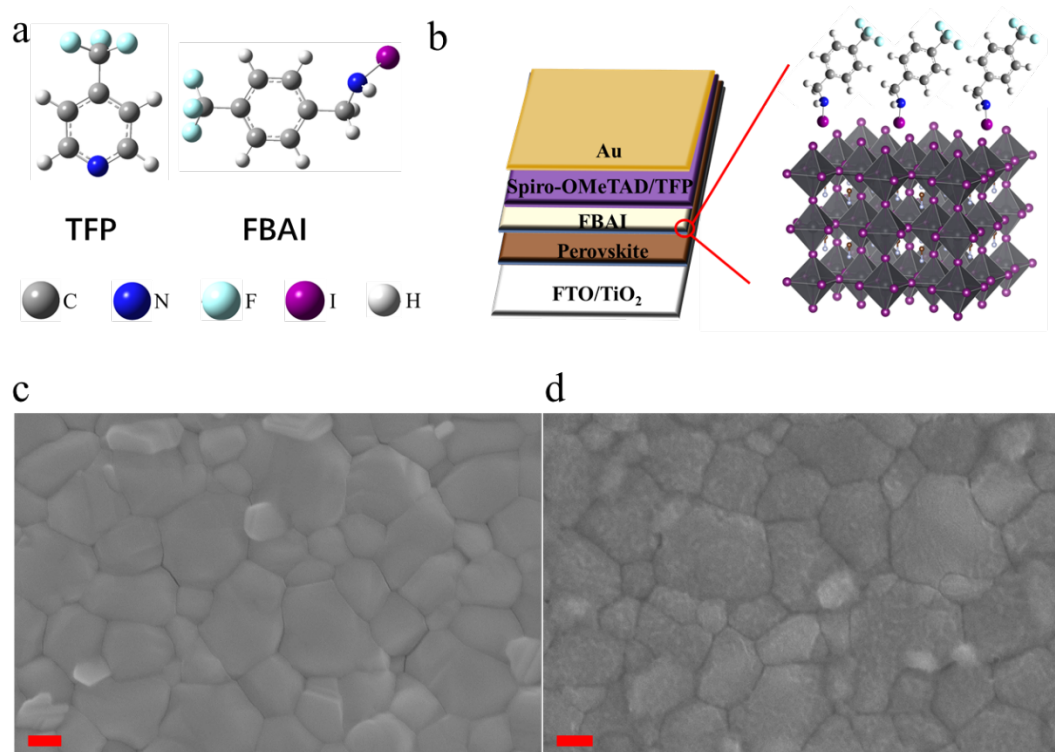
Figure 1. a) Chemical structures of TFP and FBAI. **b)** Structures of a FBAI/TFP based PSC, **c)** and **d)**, SEM images of a neat perovskite film, and a perovskite film passivated by FBAI. The scale bar is 200 nm.

FBAI Passivation

Benzylammonium iodide (BAI) and phenethylammonium iodine (PEAI) are successful passivation materials applied between perovskite/HTL interfaces[24-27]. Our previous research showed that chemically tailored passivation materials with different functional substituent groups can improve the photovoltaic performance and stability of PSCs simultaneously[23; 28]. In this study we introduce a trifluoromethyl group at the para-position of the phenyl ring in BAI (**Figure 1a**), yielding FBAI as a new passivation material. Surface morphologies of the perovskites with and without FBAI passivation are characterized by SEM and the results are shown in **Figure 1c** and **1d**. The slightly textured structure as observed in **Figure 1d** indicates formation of a top layer on the surface of the perovskite film, while the grain size does not change compared with the pristine perovskite film.

Surface and depth X-ray photoelectron spectroscopy (XPS) profiling were employed to characterize the elemental distribution and chemical environments in the perovskite films with and without FBAI passivation[29], and the results are shown in **Figure 2** and **Figure S1**. Pb 4f, F 1S and I 3d5 depth XPS profiling was used to determine the elemental distribution and thickness of the perovskite/FBAI film, and the thickness of the FBAI layer is estimated to be ~5 nm (**Figure 2a** and **2b**). The binding energies of the surface elements are shown in **Figure 2c** and **2d**. A C=O peaks at ~288 eV is clearly observed for the pristine perovskite film, referring to the interaction between the moisture or oxygen in the air and the surface of the perovskite[13]. However, the absence of such a peak for perovskite/FBAI film indicates the FBAI passivation layer can effectively protect perovskite film from decomposition caused by water and oxygen under ambient conditions. The C-F and C-N peak appearing at the perovskite/FBAI film surface belong to the FBAI molecule itself.
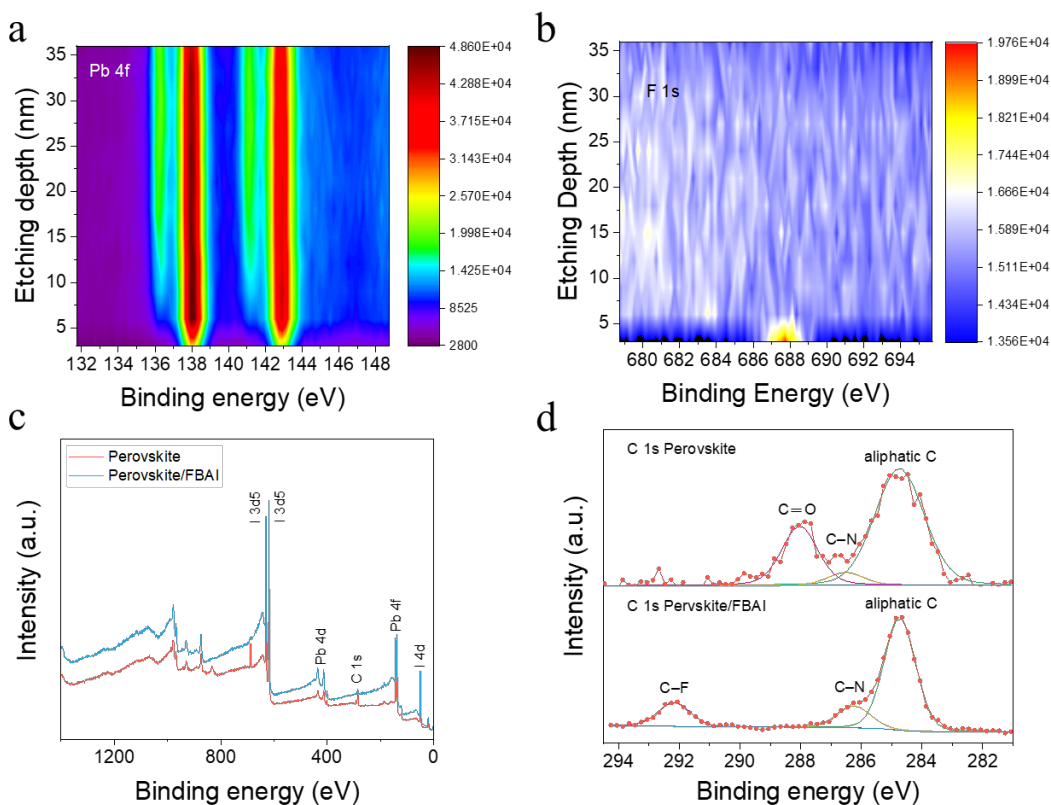
Figure 2. a-b) Pb 4f and F 1s XPS depth profiles of the perovskite/FBAI film. **c)** XPS survey spectra of neat perovskite and perovskite/FBAI films. **d)** High-resolution deconvoluted carbon 1s spectra for various films.

Structural information of the perovskite films with and without FBAI passivation is obtained by X-ray diffraction (XRD) and the results are shown in **Figure 3a**. Compared with the pristine perovskite film, the diffraction peak corresponding to excess PbI_2 for the FBAI treated perovskite disappeared, indicating that FBAI consumes the excess of lead iodide. **Figure 3b** shows the TRPL measurements of the perovskite film on FTO/Al_2O_3 substrates with and without FBAI passivation. Since the bulk film is considered to have the same non-radiative recombination rate due to the identical perovskite active layer, we attribute the slower PL decay of the FBAI passivated film to a reduction in the surface recombination rate. To quantify this, we fitted the measured TRPL traces with the model described in Zhu et al.[28], with the details of the simulations described in the Supporting Information (**Supporting Note S1**) and the results in **Table S1**. For both scenarios we obtain the same fit curves. As can be seen, FBAI passivation leads to a significant reduction of the surface recombination velocity of 115 ± 25 cm s^{-1} indicating a significantly reduced surface defect density. The surface

band structures with and without FBAI layer are measured with ultraviolet photoelectron spectroscopy (UPS) and the results are shown in **Figure S2**. The work function was determined to be −4.15 eV and −4.42 eV with the valance band maximum of −5.46 eV and −5.68 eV for perovskite and perovskite/FBAI film, respectively (**Figure 3c**). The deeper valence band bending for FBAI passivated perovskite allows to achieve a higher V_{OC} [30; 31].
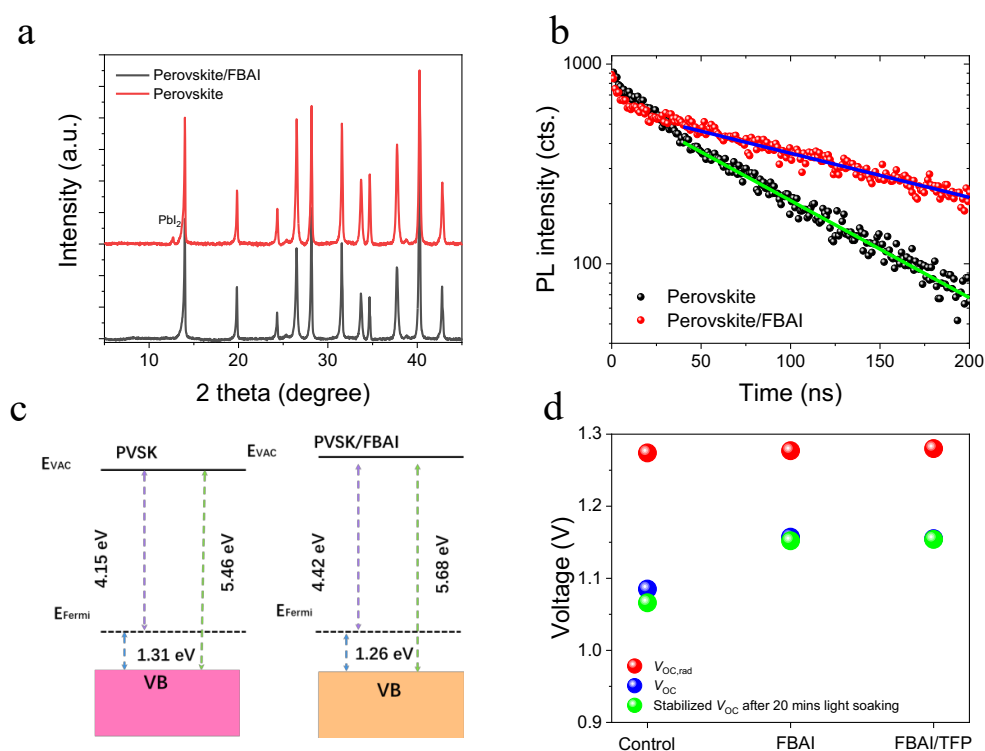
Figure 3. a) XRD patterns of neat perovskite and perovskite/FBAI films. **b)** TRPL decay and linear fit for glass/FTO/mesoscopic-Al_2O_3/perovskite with and without FBAI passivation layer **c)** Energetic diagram for neat perovskite and perovskite/FBAI films. **d)** V_{OC} and radiative limit V_{OC} for glass/FTO/compact-TiO_2/mesoscopic-TiO_2/perovskite/ (with or without) interface layer/HTL /Au. The stabilized V_{OC} after 20 min light soaking is also shown.

PLQY$_{ext}$ is used to investigate charge recombination characteristics of perovskite and perovskite/FBAI film with HTL. **Figure S4** showed that the PLQY$_{ext}$ of perovskite/FBAI is thirteen times higher than that of pristine film, implying that the FBAI layer can significantly suppress the non-radiative recombination at perovskite/spiro-OMeTAD interface. Voc losses of perovskite and perovskite/FBAI film with HTL were calculated by the equation: $\Delta V = kT \ln(PLQY)$. As shown

in **Figure 3d**, the perovskite film with FBAI layer has a theoretical V_{OC} loss as small as 90 mV compared to the counterpart pristine perovskite film exhibiting a V_{OC} loss of about 150 mV, allowing the device based on perovskite/FBAI to potentially afford a higher V_{OC}. PSCs based on perovskite/spiro-OMeTAD, perovskite/FBAI/spiro-OMeTAD and perovskite/FBAI/spiro-OMeTAD with TFP were fabricated and the radiative limits for V_{OC} ($V_{oc,rad}$) [32] (the calculation method is shown in the **Supporting Note S2**) were compared using stabilized V_{OC} (**Figure 3d)**. The smaller $V_{OC, rad}$ and V_{OC} offset shows FBAI has an outstanding defect passivation capability when compared to PSC based on neat perovskite[33]. In addition, the V_{OC} drop for FBAI and TFP based PSC is significantly lower than that of pristine PSC after 20 mins light soaking, proving that FBAI passivated layer combined with TFP dopant can increase the short-term V_{OC} stability under light soaking in ambient air.

Effect of TFP as HTL dopant

The chemical structure of TFP is shown in **Figure 1a**. TFP is derived from *t*BP where the *tert*-butyl group on *t*BP is substituted by a trifluoromethyl group. The introduction of TFP into the HTL substantially increased the resistance to moisture uptake as revealed by contact angle measurements (CAMs). As shown in **Figure S5**, the contact angle between water droplet and HTL film with varying amounts of TFP (denoted as TFP*x*, where *x* = 0.1 ~ 0.6 times the relative molar concentration of *t*BP added into the spiro-OMeTAD/*t*BP solution) increases from 70.5º to 97.5º, indicating increased hydrophobicity by the substitution of *t*BP by TFP. To verify the potential photovoltaic application of TFP in solar cell devices, PSC devices with a n-*i*-p structure of fluorine doped tin oxide (FTO)/compact TiO_2/mesoscopic TiO_2/perovskite/HTL/gold were fabricated, in which perovskite refers to a composition of $Cs_{0.05}FA_{0.85}MA_{0.10}Pb(I_{0.97}Br_{0.03})_3$ with 5% excess of PbI_2, and various amounts of TFP are introduced into the HTL. The *I-V* curves are shown in **Figure S6**, with summarized photovoltaic parameters shown in **Table S2**. Concentration screening shows that the best photovoltaic performances were obtained when *x* = 0.3, TFP concentration at which the film shows good hydrophobicity with a contact angle up to 97.6º. Surface morphologies of the HTLs with and without TFP dopant are characterized by scanning electron microscope (SEM), and the results are shown in **Figure S7**. The negligible difference between the SEM images indicates that the introduction of TFP does not affect the film morphology during the casting of HTL. Hole-

extraction and charge-recombination of the perovskite/HTLs with TFP are characterized by time-resolved photoluminescence (TRPL) and external photoluminescence quantum efficiency (PLQY$_{ext}$) measurements[34], with the later determined from the absolute intensity photon flux (AIPL) according to the methods reported by Mello et al.[35], and the results are shown in **Figure S8** and **S9**. Similar decay traces and PLQY$_{ext}$ are observed for HTL casted perovskite films with and without TFP, indicating that TFP neither compromises the extraction of holes nor alters the recombination process at perovskite/HTL interface.

Photovoltaic Performance for PSC Employing TFP and FBAI

In order to investigate the advantages of utilizing both FBAI and TFP in solar cell devices, PSCs were fabricated with a device architecture of fluorine-doped tin oxide (FTO)/compact-TiO$_2$/mesoporous TiO$_2$/perovskite (FBAI)/HTL (TFP)/gold. **Figure 4a** shows a cross-sectional SEM image of a PSC based on FBAI and TFP, with perovskite photo-absorber layer thickness of ~400 nm. *I–V* curves of these cells under 1-sun illumination are shown in **Figure 4b**, and the corresponding photovoltaic parameters are summarized in **Table 1**. The champion device based on perovskite/FBAI/TFP achieves a PCE of 23.94%, with a V_{OC} of 1163 mV, an FF of 82.4%, and a J_{SC} of 24.98 mA cm^{-2}. Such a V_{OC} represents a voltage loss of 387 mV with respect to the optical bandgap of 1.55 eV (**Figure S8** and **Figure 3d**). The V_{OC} of perovskite/FBAI/TFP based device is 64 mV higher than that of the control device and is attributed to the significantly reduced non-radiative recombination at perovskite/spiro-OMeTAD interface by the FBAI layer, which is consistent with the V_{OC} loss calculated from PLQY. The device based on perovskite/FBAI/TFP obtains a negligible hysteresis of 0.6%. In contrast, the hysteresis of the control device is 3.2%, with 20.26% PCE for forward scan and 20.90% for reverse scan. Incident photon to electron conversion efficiency (IPCE) spectra are shown in **Figure 4c**, with the integrated current densities being 24.41 mA cm^{-2} and 24.30 mA cm^{-2} for control PSC and PSC based on FBAI and TFP, respectively, which is in consistent with the J_{SC} obtain from *J-V* measurements. **Figure 4d** shows the stabilized power output at the maximum power point (MPP) for the best performing devices under 10% *r.h.* condition within the first 6 min. For the perovskite/FBAI/TFP based device the stabilized PCE is estimated to be 23.83%, which is in good agreement with the PCEs obtained from the forward and backward *J–V* scans.
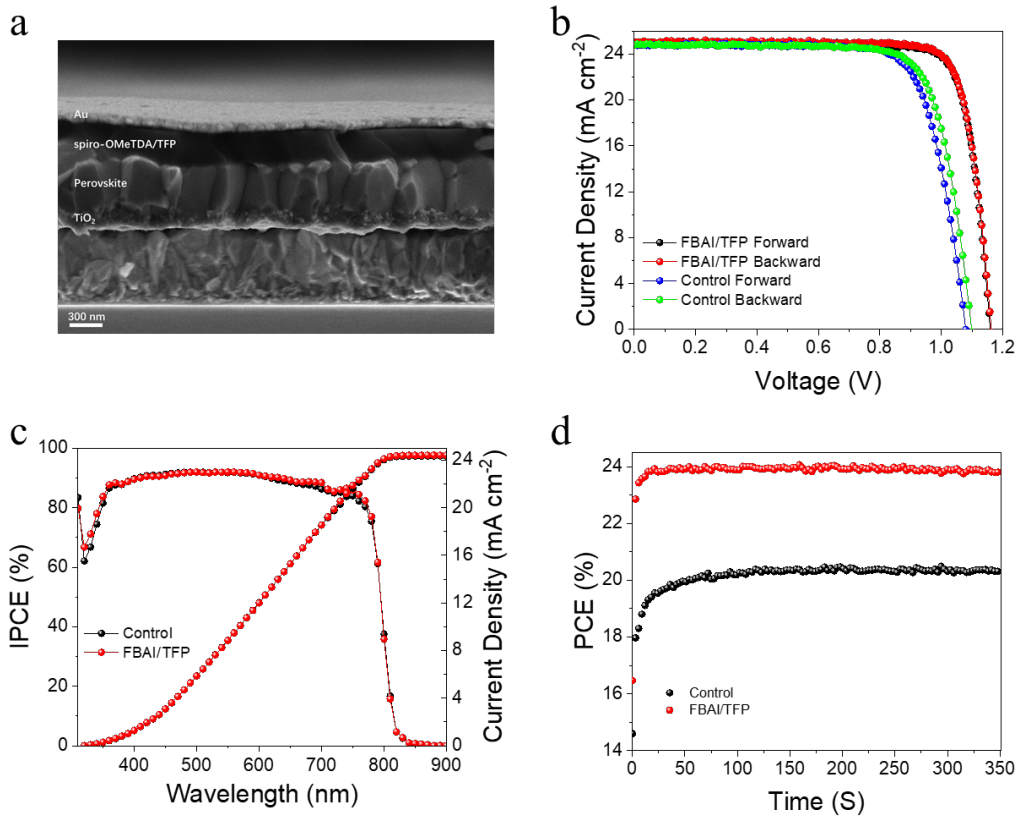
Figure 4. a) Cross-sectional SEM image of the PSC based on perovskite/FBAI/TFP. **b)** *I–V* curves of the champion PSCs. **c)** IPCE and integrated current density values of the PSCs. **d)** MPP tracking of the PSCs within the first 330 s under ambient air.

We collected the photovoltaic parameters of 20 cells in one batch based on pristine perovskite and the other based on Perovskite/FBAI/TFP cells. As shown in the **Figure 5a** and **Figure S10**, the devices based on Perovskite/FBAI/TFP show superior reproducibility as compared to the control devices. The ideality factor (n_{id}) of control PSC devices and PSC devises based on FBAI and TFP are calculated from the illumination intensity dependent V_{OC} measurements to investigate the recombination dynamics[36], and the results are shown in **Figure 5b**. The n_{id} of perovskite/FBAI/TFP is 1.57, less than that of the control device (n_{id} = 1.86), better approaching a value of n_{id} = 1. The results indicate that perovskite/FBAI/TFP devices showed slower nonradiative recombination[37], which is in good agreement with the improved photovoltaic performance for PSCs based on FBAI and TFP.

Table 1. Photovoltaic parameters of champion devices based on pristine perovskite and

perovskite/FBAI/TFP (measured under simulated AM 1.5G irradiance).

	V_{OC} (V)	J_{SC}^{a} (mA cm^{-2})	J_{SC}^{b} (mA cm^{-2})	FF	PCE (%)	MPP-PCE (%)
FBAI/TFP Backward	1.163	24.98		0.824	23.94	
			24.41			23.83
FBAI/TFP Forward	1.161	24.96		0.821	23.79	
Control Backward	1.099	24.78		0.768	20.90	
			24.30			20.36
Control Forward	1.081	24.80		0.756	20.26	

a) J_{SC} determined from the IV measurement; b) J_{SC} determined from IPCE.

Operational and environmental stability of pristine, perovskite/FBAI and perovskite/FBAI/TFP devices are evaluated. **Figure 5c** and **S11** show the operational stability results obtained with PSCs at maximum power point under 1 sun irradiation in nitrogen atmosphere (N$_2$). After 500 h, the perovskite/FBAI/TFP based PSC retains 96.5% of its initial efficiency, in contrast to 91.2% for the PSC with only FBAI interlayer and 70% for the pristine PSC. One of the reasons leading to better stability of the perovskite/FBAI/TFP based PSC devices results from a more stable FF (~ 97% compared to the control device of ~ 63%). This relatively stable FF value benefits from a more stable interface between perovskite and spiro-OMeTAD layer following passivation by FBAI[28]. Contact angle measurements of water droplets on the surface of perovskite films with and without FBAI interfacial layers are shown in **Figure S12**. The pristine perovskite and perovskite/FBAI film exhibit contact angles of 60.6° and 99.3°, respectively. These results elucidate that FBAI functions by forming a hydrophobic layer on the perovskite surface[38] to improve the stability of the perovskite. The devices based on Perovskite/FBAI/TFP show superior stability to those with FBAI passivation layer uniquely, due to an increase of hydrophobicity of spiro-OMeTAD layer (**Figure S1**) when TFP is used as additive. PSCs based on pristine, perovskite/FBAI and perovskite/FBAI/TFP devices were aged under ambient conditions with an r.h. of about 70%, and the results are shown in **Figure 5d** and **Figure S13**. It is observed that after 45 days (≈1100 h), the PCE of PSC with perovskite/FBAI/TFP declined by less than 3%, and PSC with the FBAI passivation layer only decreased by 5%, while PSCs without interface layer decreased by over 40%. The devices based on

perovskite/FBAI/TFP achieve an excellent long-term stability indicating the synergistic effect of FBAI and TFP paves a new approach to improve PSC stability.
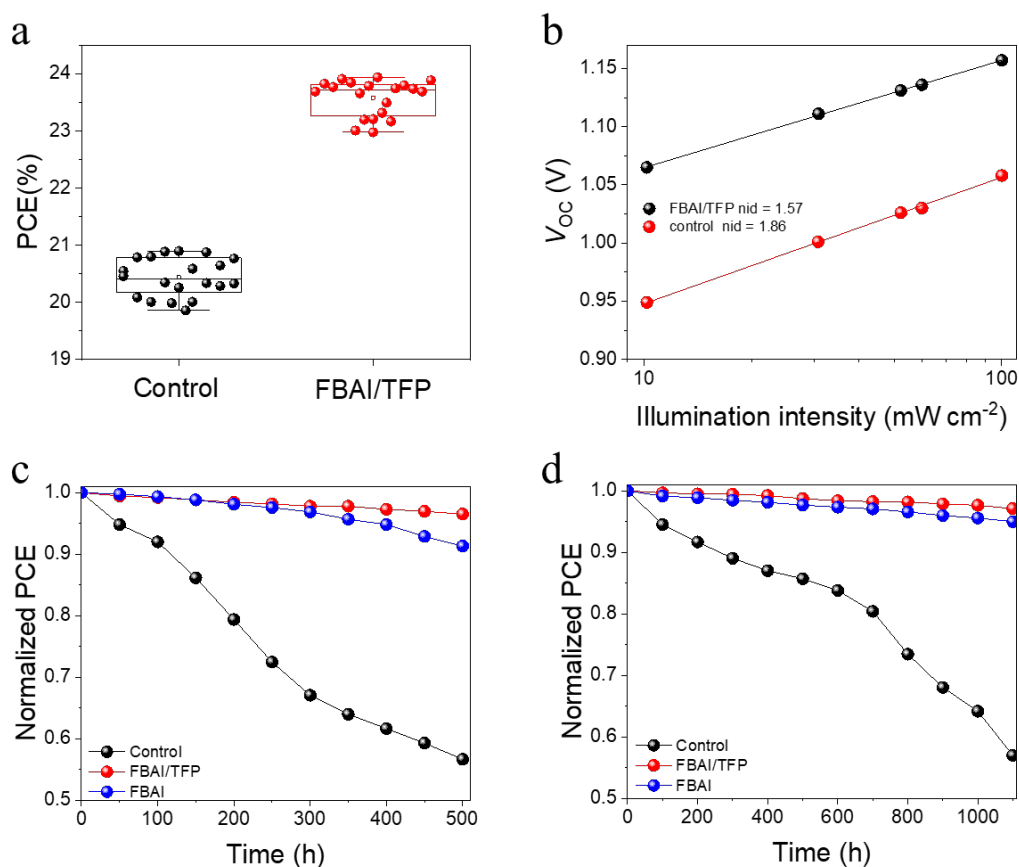
Figure 5. a) PCE distributions of 20 devices obtained from control and perovskite/FBAI/TFP device. **b)** V_{OC} as a function of light intensity of control and perovskite/FBAI/TFP devices with ideality factors (n_{id}). **c)** MPP ageing results in inert atmosphere (N_2) and under continuous 1 sun light soaking of pristine, perovskite/FBAI and perovskite/FBAI/TFP devices. **d)** Environmental stability of pristine, perovskite/FBAI and perovskite/FBAI/TFP device under a *r.h.* of about 60-70%.

Conclusion

A new strategy to improve the photovoltaic performance and operational stability of PSCs has been demonstrated. Through the synergistic effect of trifluoromethylated passivation material (FBAI) and HTL dopant (TFP), we achieve an outstanding PCE approaching 24% for PSCs with excellent long-term stability. XRD, TRPL and PLQY measurements reveal that the introduction of TFP can maintain the excellent hole extraction properties of the *state-of-the-art* spiro-OMeTAD/TBP/Li-TFSI system, while increasing the hydrophobicity of the HTL film. FBAI-passivated perovskite films also exhibit significantly suppressed nonradiative charge carrier recombination at the

perovskite/HTL interface and create a more moisture resistant interface. The champion cell based on perovskite/FBAI/TFP yielded a PCE of 23.9%, which is considered among the highest efficiencies of mesoscopic PSCs so far. In addition, the enhanced hydrophobicity of the perovskite surface and HTL layer leads to a superior resistance to moisture uptake. Remarkably, PSCs with perovskite/FBAI/TFP retain over 96.5% of their initial PCE after 500 h MPP tracking under continuous full-sun light irradiation, and over 97% of their initial PCE after 45 days under ambient air with an *r.h.* of approximately 60-70%. Our work provides an effective approach to achieve high efficiency and long-term operational stability for the advanced PSC technique.

1.   . National Renewable Energy Laboratory Best Research-Cell Efficiency Chart (National Renewable Energy Laboratory Best Research-Cell Efficiency Chart, https://www.nrel.gov/pv/cell-efficiency.html).
2.   Zhou, H., Chen, Q., Li, G., Luo, S., Song, T.-b., Duan, H.-S., Hong, Z., You, J., Liu, Y., and Yang, Y. (2014). Interface engineering of highly efficient perovskite solar cells. Science *345*, 542-546.
3.   Wang, Y., Wu, T., Barbaud, J., Kong, W., Cui, D., Chen, H., Yang, X., and Han, L. (2019). Stabilizing heterostructures of soft perovskite semiconductors. Science *365*, 687-691.
4.   Min, H., Kim, M., Lee, S.-U., Kim, H., Kim, G., Choi, K., Lee, J.H., and Seok, S.I. (2019). Efficient, stable solar cells by using inherent bandgap of α-phase formamidinium lead iodide. Science *366*, 749-753.
5.   Bai, S., Da, P., Li, C., Wang, Z., Yuan, Z., Fu, F., Kawecki, M., Liu, X., Sakai, N., Wang, J.T.-W.*, et al.* (2019). Planar perovskite solar cells with long-term stability using ionic liquid additives. Nature *571*, 245-250.
6.   Wang, Z., Shi, Z., Li, T., Chen, Y., and Huang, W. (2017). Stability of Perovskite Solar Cells: A Prospective on the Substitution of the A Cation and X Anion. Angew. Chem., Int. Ed. *56*, 1190-1212.
7.   Rong, Y., Hu, Y., Mei, A., Tan, H., Saidaminov, M.I., Seok, S.I., McGehee, M.D., Sargent, E.H., and Han, H. (2018). Challenges for commercializing perovskite solar cells. Science *361*, eaat8235.
8.   Meng, X., Zhou, J., Hou, J., Tao, X., Cheung, S.H., So, S.K., and Yang, S. (2018). Versatility of

Carbon Enables All Carbon Based Perovskite Solar Cells to Achieve High Efficiency and High Stability. Adv. Mater. *30*, 1706975.

9.   Hu, Q., Chen, W., Yang, W., Li, Y., Zhou, Y., Larson, B.W., Johnson, J.C., Lu, Y.-H., Zhong, W., Xu, J., *et al.* (2020). Improving Efficiency and Stability of Perovskite Solar Cells Enabled by A Near-Infrared-Absorbing Moisture Barrier. Joule *4*, 1575-1593.

10.   Chung, J., Shin, S.S., Kim, G., Jeon, N.J., Yang, T.-Y., Noh, J.H., and Seo, J. (2019). Impact of Electrode Materials on Process Environmental Stability of Efficient Perovskite Solar Cells. Joule *3*, 1977-1985.

11.   Kim, M., Kim, G.-H., Lee, T.K., Choi, I.W., Choi, H.W., Jo, Y., Yoon, Y.J., Kim, J.W., Lee, J., Huh, D., *et al.* Methylammonium Chloride Induces Intermediate Phase Stabilization for Efficient Perovskite Solar Cells. Joule *3*, 2179-2192.

12.   Wang, Y., Zhang, T., Kan, M., Wang, X., Zhao, Y., Dar, M.I., Gratzel, M., Ono, L.K., Qi, Y., Li, Y., *et al.* (2019). Thermodynamically stabilized β-CsPbI3-based perovskite solar cells with efficiencies >18. Science *365*, 591-595.

13.   Jiang, Q., Zhao, Y., Zhang, X., Yang, X., Chen, Y., Chu, Z., Ye, Q., Li, X., Yin, Z., and You, J. (2019). Surface passivation of perovskite film for efficient solar cells. Nat. Photonics *13*, 460-466.

14.   Bu, T., Li, J., Zheng, F., Chen, W., Wen, X., Ku, Z., Peng, Y., Zhong, J., Cheng, Y.-B., and Huang, F. (2018). Universal passivation strategy to slot-die printed SnO2 for hysteresis-free efficient flexible perovskite solar module. Nat. Commun. *9*, 1-10.

15.   Zhang, F., Yao, Z., Guo, Y., Li, Y., Bergstrand, J., Brett, C.J., Cai, B., Hajian, A., Guo, Y., Yang, X., *et al.* (2019). Polymeric, Cost-Effective, Dopant-Free, Hole Transport Materials for Efficient and Stable Perovskite Solar Cells. J. Am. Chem. Soc. *141*, 19700-19707.

16.   Liao, H.-C., Tam, T.L.D., Guo, P., Wu, Y., Manley, E.F., Huang, W., Zhou, N., Soe, C.M.M., Wang, B., Wasielewski, M.R., *et al.* (2016). Dopant-Free Hole Transporting Polymers for High Efficiency, Environmentally Stable Perovskite Solar Cells. Adv. Energy Mater. *6*, 1600502.

17.   Yang, J., Liu, C., Cai, C., Hu, X., Huang, Z., Duan, X., Meng, X., Yuan, Z., Tan, L., and Chen, Y. (2019). High-Performance Perovskite Solar Cells with Excellent Humidity and Thermo-Stability via Fluorinated Perylenediimide. Adv. Energy Mater. *9*, 1900198.

18.   Kim, J.-E., Kim, S.-S., Zuo, C., Gao, M., Vak, D., and Kim, D.-Y. (2019). Humidity-Tolerant Roll-to-Roll Fabrication of Perovskite Solar Cells via Polymer-Additive-Assisted Hot Slot Die Deposition. Adv. Funct. Mater. 10.1002/adfm.201809194,

19.   Zhang, J., Zhang, T., Jiang, L., Bach, U., and Cheng, Y.-B. (2018). 4-tert-Butylpyridine Free Hole Transport Materials for Efficient Perovskite Solar Cells: A New Strategy to Enhance the Environmental and Thermal Stability. ACS Energy Lett. *3*, 1677-1682.

20.   Hawash, Z., Ono, L.K., and Qi, Y. (2018). Recent Advances in Spiro-MeOTAD Hole Transport Material and Its Applications in Organic-Inorganic Halide Perovskite Solar Cells. Adv. Mater. Interfaces *5*, 1700623.

21.   Schloemer, T.H., Christians, J.A., Luther, J.M., and Sellinger, A. (2019). Doping Strategies for Small Molecule Organic Hole-Transport Materials: Impacts on Perovskite Solar Cell Performance and Stability. Chem. Sci. 10.1039/c8sc05284k,

22.   Jena, A.K., Ikegami, M., and Miyasaka, T. (2017). Severe Morphological Deformation of Spiro-OMeTAD in (CH3NH3)PbI3 Solar Cells at High Temperature. ACS Energy Lett. 10.1021/acsenergylett.7b00582,

23.   Liu, Y., Akin, S., Uchida, R., Arora, N., Milic, J.V., Uhl, A.R., Zakeeruddin, S.M., Dar, M.I., Gratzel,

M., Akin, S., *et al.* (2019). Ultrahydrophobic 3D/2D fluoroarene bilayer-based water-resistant perovskite solar cells with efficiencies exceeding 22. Sci. Adv. *5*, eaaw2543.

24.   Zhou, Y., Wang, F., Cao, Y., Wang, J.-P., Fang, H.-H., Loi, M.A., Zhao, N., and Wong, C.-P. (2017). Benzylamine-Treated Wide-Bandgap Perovskite with High Thermal-Photostability and Photovoltaic Performance. Adv. Energy Mater. 10.1002/aenm.201701048,

25.   Gao, F., Zhao, Y., Zhang, X., and You, J. (2019). Recent Progresses on Defect Passivation toward Efficient Perovskite Solar Cells. Adv. Energy Mater. 10.1002/aenm.201902650,

26.   Chen, B., Rudd, P.N., Yang, S., Huang, J., and Yuan, Y. (2019). Imperfections and their passivation in halide perovskite solar cells. Chem Soc Rev.

27.   Liu, C., Masse, R., Jia, X., Bi, W., Neale, Z., Xu, M., Tian, M., Zheng, J., Cao, G., Yuan, J., *et al.* (2020). Interphases, Interfaces, and Surfaces of Active Materials in Rechargeable Batteries and Perovskite Solar Cells. Adv Mater, e1905245.

28.   Zhu, H., Liu, Y., Eickemeyer, F.T., Pan, L., Ren, D., Ruiz-Preciado, M.A., Carlsen, B., Yang, B., Dong, X., Wang, Z., *et al.* (2020). Tailored Amphiphilic Molecular Mitigators for Stable Perovskite Solar Cells with 23.5% Efficiency. Adv. Mater. *32*, 1907757.

29.   Wang, R., Xue, J., Meng, L., Lee, J.-W., Zhao, Z., Sun, P., Cai, L., Huang, T., Wang, Z., Wang, Z.-K., *et al.* (2019). Caffeine Improves the Performance and Thermal Stability of Perovskite Solar Cells. Joule *3*, 1464-1477.

30.   Jiang, Q., Ni, Z., Xu, G., Lin, Y., Rudd, P.N., Huang, J., Xu, G., Xue, R., Li, Y., Li, Y., *et al.* (2020). Interfacial Molecular Doping of Metal Halide Perovskites for Highly Efficient Solar Cells. Adv Mater, e2001581.

31.   Wang, R., Xue, J., Wang, K.-L., Wang, Z.-K., Luo, Y., Fenning, D., Xu, G., Nuryyeva, S., Huang, T., Zhao, Y., *et al.* (2019). Constructive molecular configurations for surface-defect passivation of perovskite photovoltaics. Science (Washington, DC, U. S.) *366*, 1509-1513.

32.   Krueckemeier, L., Rau, U., Stolterfoht, M., and Kirchartz, T. (2020). How to Report Record Open-Circuit Voltages in Lead-Halide Perovskite Solar Cells. Adv. Energy Mater. *10*, 1902573.

33.   Luo, D., Su, R., Zhang, W., Gong, Q., and Zhu, R. (2019). Minimizing non-radiative recombination losses in perovskite solar cells. Nat. Rev. Mater. 10.1038/s41578-019-0151-y,

34.   Zhang, S., Hosseini, S.M., Gunder, R., Petsiuk, A., Caprioglio, P., Wolff, C.M., Shoaee, S., Meredith, P., Schorr, S., Unold, T., *et al.* (2019). The Role of Bulk and Interface Recombination in High-Efficiency Low-Dimensional Perovskite Solar Cells. Adv. Mater. 10.1002/adma.201901090,.

35.   de Mello, J.C., Wittmann, H.F., and Friend, R.H. (1997). An improved experimental determination of external photoluminescence quantum efficiency. Adv. Mater. *9*, 230-232.

36.   Kong, X., Jiang, Y., Wu, X., Chen, C., Guo, J., Liu, S., Gao, X., Zhou, G., Liu, J.-M., Kempa, K., *et al.* (2020). Dopant-free F-substituted benzodithiophene copolymer hole-transporting materials for efficient and stable perovskite solar cells. J. Mater. Chem. A *8*, 1858-1684.

37.   Cai, M., Ishida, N., Li, X., Yang, X., Noda, T., Wu, Y., Xie, F., Naito, H., Fujita, D., and Han, L. (2018). Control of Electrical Potential Distribution for High-Performance Perovskite Solar Cells. Joule 10.1016/j.joule.2017.11.015, t.

38.   Liu, Y., Akin, S., Hinderhofer, A., Eickemeyer, F.T., Zhu, H., Seo, J.-Y., Zhang, J., Schreiber, F., Zhang, H., Zakeeruddin, S.M., *et al.* (2020). Stabilization of Highly Efficient and Stable Phase-Pure FAPbl3 Perovskite Solar Cells by Molecularly Tailored 2D-Overlayers. Angew. Chem., Int. Ed. 10.1002/anie.202005211, 15688.